Investigation of the interaction between adsorbed water and various morphologies of boehmite nanoparticles prepared by continuous supercritical hydrothermal synthesis

Erwan Peigney, Angeline Poulon-Quintin, Marjorie Cavarroc, Guillaume Aubert, Mathieu Duttine, Christine Labrugère Sarroste, Cyril Aymonier

To cite this version:

Erwan Peigney, Angeline Poulon-Quintin, Marjorie Cavarroc, Guillaume Aubert, Mathieu Duttine, et al.. Investigation of the interaction between adsorbed water and various morphologies of boehmite nanoparticles prepared by continuous supercritical hydrothermal synthesis. Journal of Supercritical Fluids, 2023, 193, 105829 (11 p.). 10.1016/j.supflu.2022.105829 . hal-03907821

HAL Id: hal-03907821
https://hal.science/hal-03907821

Submitted on 20 Dec 2022

Investigation of the interaction between adsorbed water and various morphologies of boehmite nanoparticles prepared by continuous supercritical hydrothermal synthesis.

Erwan Peigney [a], Angéline Poulon-Quintin [a,*], Marjorie Cavarroc [b], Guillaume Aubert [a], Mathieu Duttine [a], Christine Labrugère Sarroste [c], Cyril Aymonier [a,*]

[a] *Univ. Bordeaux, CNRS, Bordeaux INP, ICMCB, UMR 5026, F-33600 Pessac, France*

[b] *SAFRAN Tech, Châteaufort, CS 80112, 78772 Magny-les-Hameaux, France*

[c] *Univ. Bordeaux, CNRS, PLACAMAT, UAR 3626, F-33600 Pessac, France*

* corresponding author:cyril.aymonier@icmcb.cnrs.fr (Cyril Aymonier) and angeline.poulon@icmcb.cnrs.fr (Angéline Poulon-Quintin).

Abstract

Boehmite applications are often subject to specific characteristics in terms of morphologies and surface properties. The versatile continuous supercritical hydrothermal method allows synthesizing various boehmite morphologies from rhombic to hexagonal platelet-like nanoparticles depending on the preferential adsorption of part of the precursor after transformation species on the (020) surface resulting in a preferential growth along [001] and mostly [100] directions. This adsorption on surface free sites plays the role of morphology stabilizer and results in the reduction of adsorbed water.

The interaction between adsorbed water and the boehmite morphology depends on various parameters; 1) the structure order of boehmite as exhibited by XPS analysis associated with ^{1}H Solid-State NMR spectroscopy and, 2) the number of available free sites, which tend to be filled by the adsorption of nitrates as observed by Raman spectroscopy.

Keywords: Synthetic boehmite nanoparticles; Water and nitrate adsorption; pH-dependent morphology; Continuous supercritical hydrothermal synthesis; Supercritical water.

1. Introduction

An explosion of research works on nanotechnologies has marked the last decade. In particular, inorganic nanoparticles are of interest in broad domains ranging from electronics to pharmaceuticals. These fields require high performance crystallized materials with controlled sizes and morphologies. Additionally, industrial scale applications need low-price, reproducibility and environmentally friendly conditions to meet society challenges [1]. This can be achieved through continuous supercritical hydrothermal synthesis [2].

Boehmite, an aluminium oxyhydroxide (γ-AlOOH), is widely used as catalyst [3], adsorbent [4–6], coating [7], membrane [8] and fire-retardant [9]. Furthermore, it is an important precursor for the preparation of aluminium oxides such as ϒ-, θ-, χ-, κ- and α-$\mathrm{Al_2O_3}$ [10].

Boehmite has an orthorhombic crystal structure (space group *Cmcm*), shown on Figure 1, characterized by double sheets of distorted edge-sharing octahedra with oxygen atoms at the top and aluminium ones at the centre. These double layers are linked together by hydrogen

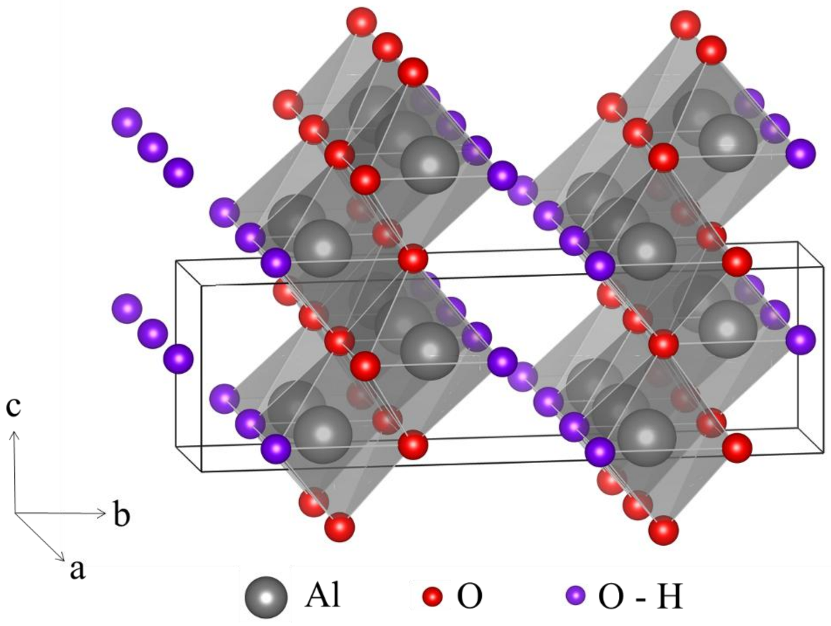

Figure 1: Schematic representation of two unit cells of orthorhombic crystal structure of boehmite.

bonds forming parallel rows of chains in zig-zag perpendicular to the b-axis.

Because of the weak interaction, the crystal surface ends in the interface between two double layers. This produces surfaces full of hydroxyl groups [11,12]. Consequently, boehmite nanoparticles tend to have a large excess of adsorbed water up to 30 wt.%, leading to the name of "pseudo-boehmite" [13]. At first, the literature hypothesized that this adsorbed water was incorporated in the sheet interlayer along the b-axis [14]. The lattice deformation along this specific axis appears to be insufficient to insert water molecules which are considered to be only adsorbed on the boehmite surfaces [15].

The structure tends to show platelet-like particles with a dominant (010) basal surface and less stable (100), (101) and (001) edge facets. A Density Functional Theory (DFT) study of boehmite surface properties exhibited the basal (010) surface forms about 50 % of the total surface [16]. This surface is characterized by the smallest interfacial energy and a weak chemical reactivity with water. That is why water is mainly physisorbed on it.

The relative surfaces of each facet can be modified through the synthesis route, which may influence the adsorbed water content. The morphology of boehmite particles can be easily tuned thanks to the versatility of the continuous supercritical hydrothermal synthesis method. Adschiri *et al.* have reported for the first time the use of this technique for the preparation of boehmite [17] which, was traditionally synthesized using sol-gel precipitation or hydrothermal synthesis [18,19]. They showed the influence of various parameters such as temperature, pressure, pH and precursor concentration on the particle characteristics. Hakuta *et al.* were able, with a hydrothermal process, to modify the shape of boehmite particles from hexagonal platelet-like to rhombic shaped by increasing the temperature from 350 °C to 400 °C [20]. More recently, Fujii *et al.* demonstrated the ability of alkylcarboxylic acids to change the aspect ratio of boehmite particles up to 5-fold [21]. They suggested that carboxylic acid inhibits crystal growth along the [001] and [010] axes relative to the [100] direction through surface-capping, resulting in the formation of rodlike particles. The variation of the particle morphology necessarily generates an evolution of the active surfaces, the surface properties and thus of the potential quantity of adsorbed water. All of which play a crucial role in the final material properties and thus performance for applications where boehmite is used and need to be investigated.

This paper reports the ability of supercritical boehmite γ-AlOOH surfaces to interact with water. Supercritical boehmite particles were synthesized using the continuous supercritical hydrothermal process. Microstructures were determined by Rietveld analysis of Powder X-Ray Diffraction (PXRD) data and Transmission Electron Microscopy (TEM). Adsorbed water was investigated using X-Ray Photoelectron Spectroscopy (XPS), ^{1}H Solid-State Nuclear Magnetic Resonance (NMR) and Raman Spectroscopy.

2. Experimental

2.1 Materials

Boehmite particles were prepared using the continuous supercritical hydrothermal synthesis. Aluminium nitrate nonahydrate $Al(NO_3)_3{\cdot}9H_2O$ (> 98 % purity) was selected as precursor. The metal salt was dissolved into distilled water (10-18 MΩ.cm). Sodium hydroxide NaOH (> 98 % purity) was used to increase the pH of the precursor solution from 3.9 up to 6.7. All the chemicals were purchased from Sigma-Aldrich and used as received.

2.2 Hydrothermal flow synthesis apparatus and procedure

Continuous flow synthesis was carried out in a homemade reactor custom-designed to minimize clogging problems. It is made of a 0.74 m long stainless steel pipe with an internal diameter of 4.78 mm. The set-up consists of a HPLC pump, two ceramic band heaters and a

TESCOM back pressure regulator. This equipment has been thoroughly described elsewhere [22].

The reactor is first pressurized to 25 MPa at ambient temperature using distilled water and then set to the process temperature of 400 °C. Precursor solution is fed at a flow rate of 3.5 or 6.6 $mL.min^{-1}$ corresponding to residence times of 60 s and 20 s, respectively. At the outlet of the reactor, the chemical reaction is stopped by ice bath quenching. A stainless steel fritted filter is placed inside the quenching system to collect the produced nanoparticles. The product is recovered as a gel, which is washed several times with distilled water. Produced powders were then dried in an oven at 60 °C overnight.

2.3 Material characterization

2.3.1 Powder X-Ray Diffraction (PXRD)

Powder X-Ray Diffraction (PXRD) patterns were collected at room temperature on a PANalitycal X'pert PRO MPD diffractometer with the Bragg−Brentano $\theta-2\theta$ geometry and over a 2θ angular range from 10 ° to 130 ° (minimum step of 0.008 °). The diffractometer was equipped with a Ge (111) monochromator, which generated a perfectly Cu $K\alpha_1$ radiation (λ = 1.540598 Å) at 45 kV and 40 mA. A multichannel X'Celerator detector was used to collect the XRD patterns. Prior to measurement, samples were finely ground to break up the aggregates and passed through a 50 μm mesh sieve. Afterward, powder was placed and randomly distributed on a silicone sample holder.

2.3.2 Rietveld refinement

Data were analysed by Rietveld structural model refinements using the FullProf Suite software package [23]. The Thompson−Cox−Hasting formulation of the pseudo-Voigt function was used to fit the Bragg reflection. Refined parameters were the 8-coefficient polynomial functions of background, instrumental zero, scale factor, unit cell parameters, Gaussian and Lorentzian contributions and microstructural strain parameters. The model included only the Al and O atom positions and isotropic thermal parameters. Crystallite shape anisotropy, specific to boehmite particles, was taken into account through spherical harmonic functions. Up to six harmonics were used to describe size broadening for the orthorhombic structure [24]. Simulated X-ray diffractogram quality was measured with the weighted-profile *R*-factor (R_{wp}).

2.3.3 Transmission Electron Microscopy (TEM)

The boehmite particle morphology was investigated using Transmission Electron Microscopy (TEM) with a ThermoFisher Talos F200S G2 microscope. Micrographs were captured with an electron beam voltage of 200 keV allowing an accessible range of magnification up to x1,050,000 and a resolution of 0.1 Å. Prior to the observation, less than 2 mg of powder were put in ethanol (≈ 1 mL) and dispersed with ultrasound during 5 min. Then, TEM thin foils were prepared by drop casting the solution made beforehand onto a holey carbon-coated grid and dried at room temperature.

2.3.4 X-Ray Photoelectron Spectroscopy (XPS)

XPS spectra of boehmite were collected with a ThermoFisher Scientific K-Alpha spectrometer using a monochromatic Al Kα X-radiation (1486.6 eV) and a hemispherical electron energy analyser. Powder was pressed onto indium foil fixed on a metallic support. This technique was used to characterize extreme surfaces of a set of grains (*i.e.* about 3 to 5 nm in depth) with a 400 µm diameter X-Ray spot size. The binding energies reported were referenced with the C_{1s} peak at 284.9 eV. Survey and the high-resolution spectra Al_{2p}, O_{1s}, and C_{1s} are reported. Elemental composition was calculated from areas of high-resolution spectra acquired with a pass energy of 40 eV. Experimental data were curve fitted into components with Gaussian-Lorentzian peaks using the ThermoFisher Scientific *Avantage* software.

2.3.5 Raman Spectroscopy

The vibrational properties of boehmite were characterized by a Raman spectrometer Horiba LaBRAM HR Evolution. Spectra were acquired with a 532 nm laser wavelength and a spot size of 1 µm. Boehmite particles dispersed in ethanol were drop-casted onto a glass slide and air dried during one day. Before each analysis, the spectrometer was calibrated using the 520.5 cm^{-1} peak of Si acquired on a silicon wafer. The measurements were performed with a long working distance x100 objective lens, a 600 lines/mm grating and a CCD detector. Acquisitions were done for an exposure time of 20 s. Each spectrum was accumulated 40 times to optimize the signal-to-noise ratio on the 200 – 1200 and 2900 – 3800 cm^{-1} ranges to visualize the major bands of boehmite with the hydroxyl deformation modes located at 360, 495 and 674 cm^{-1}, the hydroxyl stretching bands at 3085 and 3220 cm^{-1} and any remaining water beyond [25]. The aluminium nitrate band is mainly located at 1049 cm^{-1} [26].

2.3.6 Solid-State Nuclear Magnetic Resonance Spectroscopy

^1H Solid-State Nuclear Magnetic Resonance (NMR) analyses were carried out on a Bruker Avance III 300 WB spectrometer (B0 = 7.05 T). Experiments were performed with a 2.5 mm solid probe under Magic Angle Spinning (MAS) conditions (30 kHz) with a rotor-synchronized Hahn-echo pulse sequence (90 ° - 180 °) with a 90 ° pulse length of 2 µs and an optimized recycle delay of 5 s. The chemical shift scale was calibrated using H_2O milliQ ($\delta(^1H) = + 4.7$ ppm) as reference. Desummation of the ^1H MAS NMR spectra was performed with *Dmfit* software [27].

3. Results

3.1 Influence of the process operating parameters on the grain morphologies

Influence of different operating parameters on the hydrothermal flow synthesis of boehmite was widely reported in the literature [17,20,28]. pH is one of the major parameters to modify the boehmite particle morphology without adding additives. Using aluminium nitrate as precursor, pH variation can be achieved by: 1) adjusting the precursor concentration and, 2) adding NaOH.

The syntheses were performed at 25 MPa, 400 °C and for different pH values 2.9, 3.5, 3.9 by varying the nitrate concentration and at pH = 6.7 by adding NaOH. In this article, these samples are labelled S2.9, S3.5, S3.9 and S6.7, respectively. Table 1 summarizes process operating parameter variations we used. The residence time was fixed at 20 s except for S3.5 with 60 s as residence time.

Table 1: Process operating parameters for the boehmite syntheses performed at 25 MPa and 400 °C.

Sample name	S2.9	S3.5	S3.9	S6.7
Residence time (s)	20	60	20	20
Precursor concentration (mol.L^{-1})	1.10^{-1}	2.10^{-2}	5.10^{-3}	2.10^{-2}
pH	2.9	3.5	3.9	6.7

Morphology of the as-synthesized particles was investigated using TEM analysis. As shown in Figure 2, boehmite particles are anisotropic. S2.9 and S3.5 powders exhibit strongly aggregated hexagonal particles of about a few hundred nanometers in length (Figure 2a) and b)). The particles are very thin, less than 15 nm as observed on TEM images of S3.5 and S3.9 (Figure 2b) and c)). The increase of the residence time from 20 to 60 s does not seem to favour the particle growth. This has already been observed by Hakuta *et al.* who assumed the particles grow only at the very early stage of the reaction (< 2 s) at 25 MPa and 400 °C in acidic conditions [20].

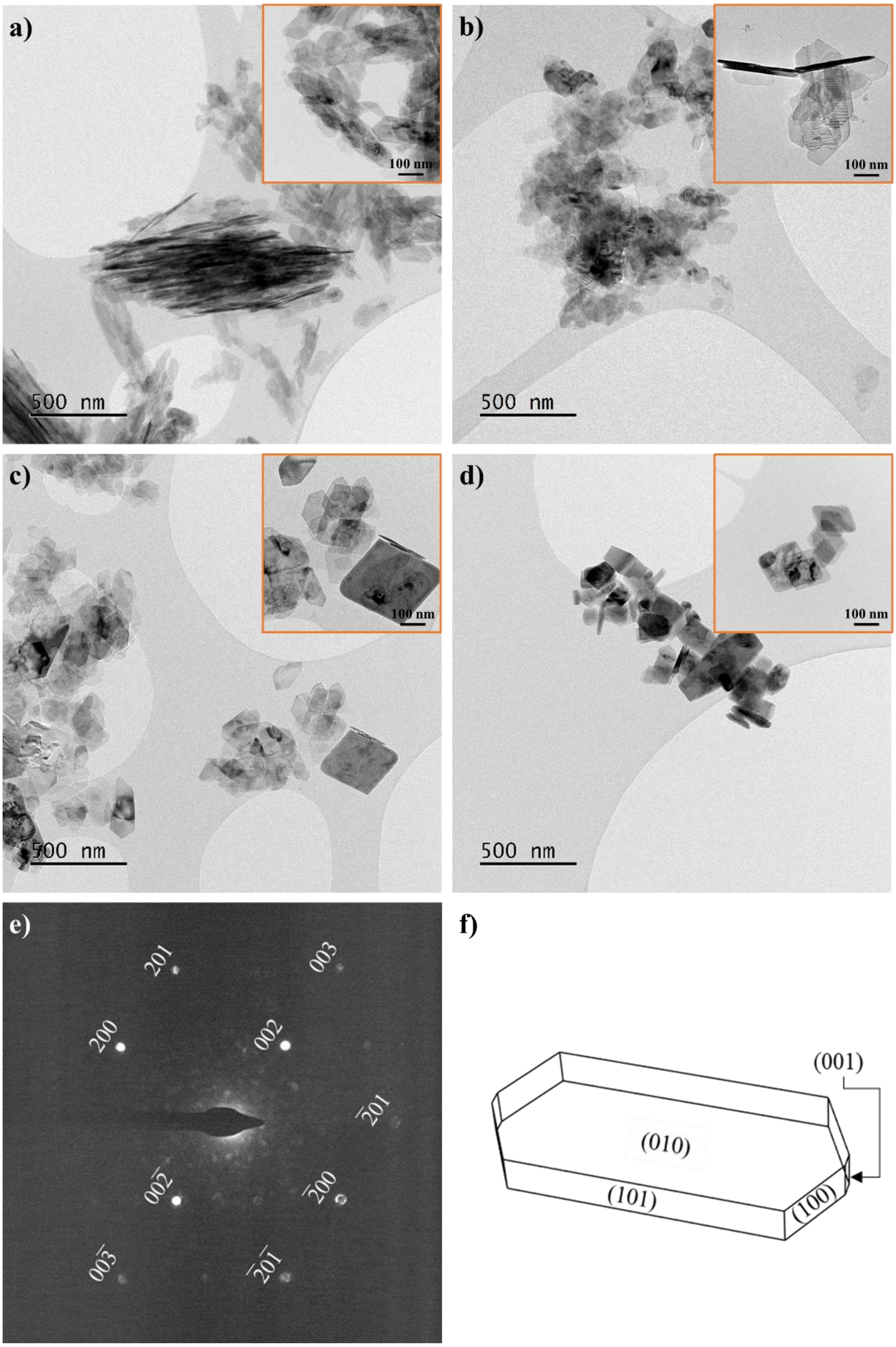

Figure 2: TEM images of boehmite particles: a) S2.9, b) S3.5, c) S3.9 and d) S6.7 associated with the electron diffraction pattern of a hexagonal particle of S3.9 on e) and a scheme of a hexagonal platelet grain on f).

A further increase of the pH value results in the formation of rhombic particles. S3.9 powder shows both aggregated hexagonal and rhombic particles. Moving to a near neutral pH allows the synthesis of perfectly rhombic boehmite particles. Alkaline pH of 9.3 and 12.0 were also tested, but are not presented here. Slightly basic conditions gave a mix of boehmite and bayerite, an aluminium hydroxide α-$Al(OH)_3$ whereas strong basic ones did not produce any particles. This is in agreement with Hakuta *et al.* observations [20]. They explained the particle disappearance by a redissolution of very small particles during cooling. However, recent research brings new hypotheses with the discovery of Hydrothermal Molten Salts (HyMOS) [29]. The precipitation at a higher temperature than their melting point *i.e.* between 318 and 323 °C for NaOH is instantaneously followed by the fusion of the salts. It produces a unique system composed of supercritical water at low density with a fraction of dissolved salt and a molten salt phase with a fraction of water [30]. The high polarity and density of molten salts results in dissolving a large amount of inorganic particles that could be the case of boehmite. Voisin et al. [29] demonstrated the formation of NaOH molten salts in supercritical water at 400 °C and 25 MPa. One of the conditions for observing molten salt is the prior NaOH precipitation (before melting) meaning that a salt concentration above its solubility (133 ppm at 400 °C and 25 MPa) is necessary. In this study, this condition is achieved with a NaOH concentration of 400 ppm approximately at a pH of 12. Although molten salts have never been observed under these specific conditions, all conditions required to obtain them are met and could also explain the redissolution of boehmite nanoparticles. Zhang *et al.* discussed the effect of pH on the growth of boehmite using traditional hydrothermal synthesis based on sol-gel process. In their study, a pH higher than 12 is required to obtain rhombic grains [31]. The [010] zone axis electron diffraction pattern in Figure 2e) reveals diffraction spots of (100), (001) and (101) planes. Such a result is consistent with a hexagonal grain with a dominant (020) surface and (100), (001) and (101) edge surfaces as represented on the scheme shown in Figure 2f).

The aggregation makes particle size determination complex. To overcome this issue, boehmite particles are then defined by their Average Crystallite Size (A.C.S). X-ray

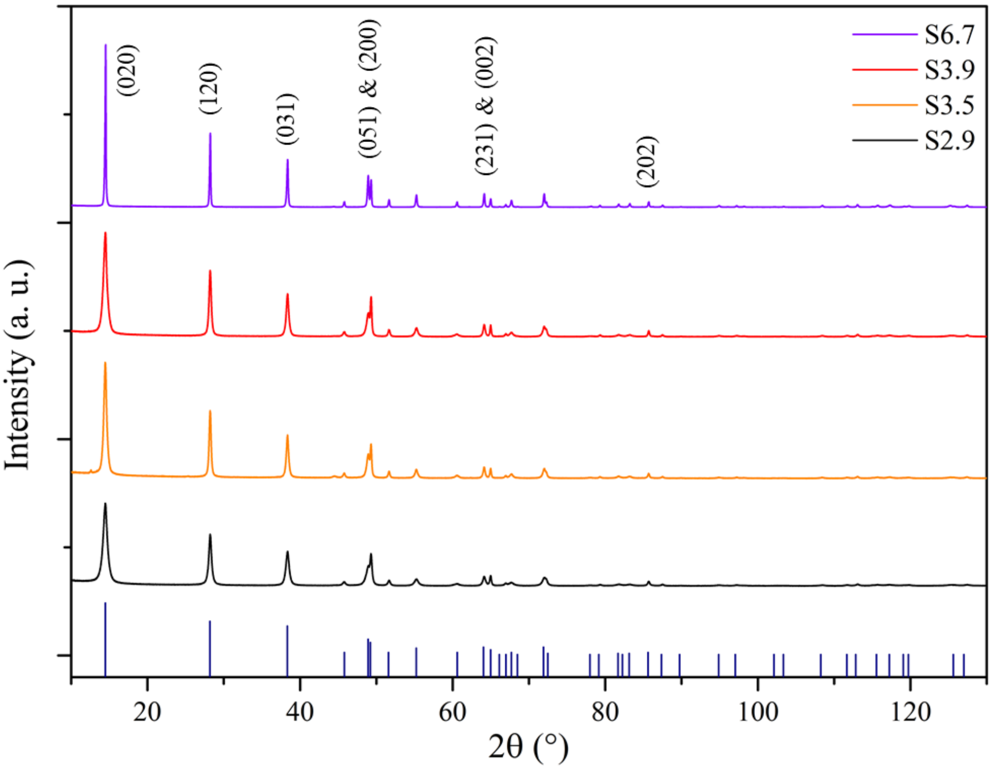

Figure 3: X-ray diffraction patterns of the four studied samples. In blue, boehmite peak positions and their theoretical intensities from the PDF file # 00-021-1307.

diffraction patterns of the as-synthesized powder are shown in Figure 3. They confirmed the synthesis of well-crystallized boehmite powders independently of the pH value. Using the PDF # 00-021-1307 file for an orthorhombic boehmite (space group *Cmcm*), plan identification of boehmite is assigned in Figure 3. Crystallized boehmite is described by a most intense (020) peak (2θ = 14.5 °) followed by (021) (2θ = 28.2 °) and (130) (2θ = 38.4 °) peaks of half the intensity.

A deep study of the crystal structure is proposed by simulating the experimental X-ray diffraction patterns thanks to the Rietveld refinement method. An example for the S2.9 sample is displayed in Figure 4. The accuracy of the Rietveld refinement presented is relatively good with a weighted-profile R-factor of 9%. Refined crystal parameters for all the studied powders are reported in Table 2.

Refined lattice parameters, and especially along the b-axis, do not show significant discrepancies showing that no atom or water molecule could be inserted within the structure. Guzmán-Castillo *et al.* have also made this observation [15]. As expected for anisotropic particles, peak broadening varies from peak to peak. In agreement with the scheme of a hexagonal grain and the electron diffraction pattern (Figure 2e) and f)), boehmite particles can be characterized by the (200), (020), (002) and (202) diffraction peaks observed at 49.3°, 14.5°, 65.0° and 85.7°, respectively.

The assumption of a parallelepipedic grain is done by taking into account the crystallite dimensions only along the [100], [010] and [001] directions to facilitate the study. Table 2

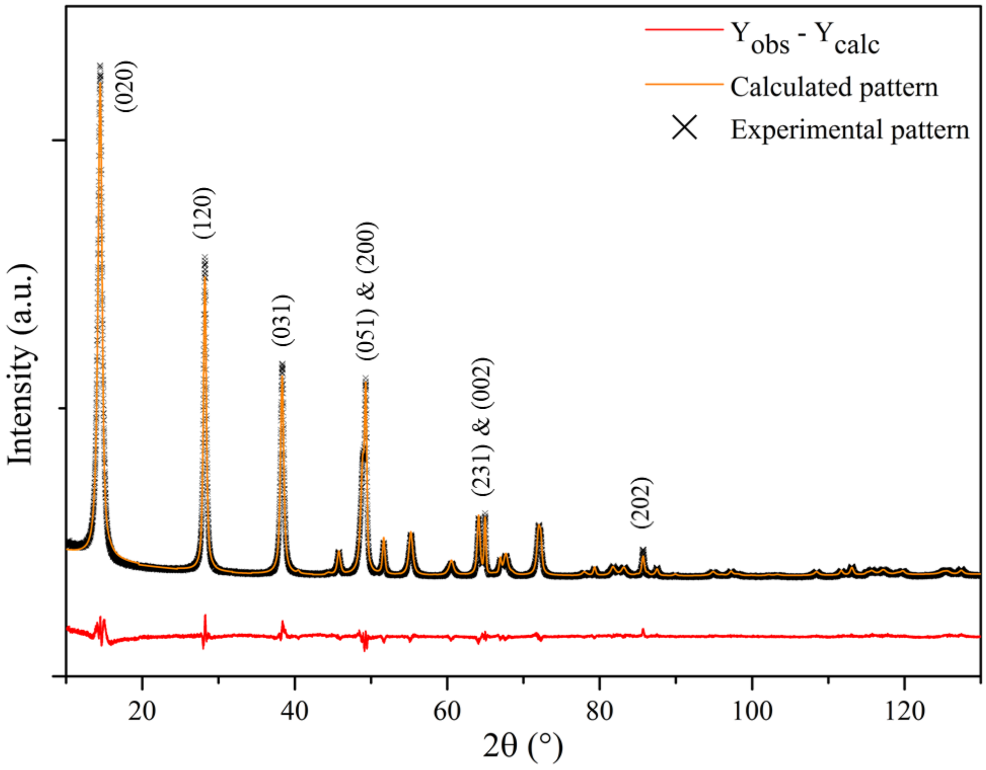

Figure 4: Rietveld refinement plot performed for the S2.9 X-ray diffraction pattern.

discloses estimated average crystallite dimensions using full width at half maximum (FWHM) from refinement output labelled l_{200}, l_{020} and l_{002} along the [100], [010] and [001] directions. A.C.S. reported through Rietveld refinement are smaller than qualitative observations performed on the TEM images, which confirmed the polycrystalline nature of the powders. In contrast, the l_{020} length corresponds approximately to the measurements done on the crystallite thicknesses shown in Figure 2b) and c) for S3.5 and S3.9, respectively. These particles oriented parallel to the b-axis exhibit thicknesses less than 15 nm fitting with the 12 and 10 nm values estimated from Rietveld refinement. It suggests that polycrystalline particles are made of a unique layer of crystallites perpendicularly aligned to the b-axis.

S6.7 powder presents relatively large crystallites compared to the three others (at least twice the size along all crystallographic directions). For instance, S2.9 has l_{200}, l_{020} and l_{002} of 28 ± 5 nm, 10 ± 2 nm and 23 ± 6 nm while those of S6.7 are 47 ± 4 nm, 39 ± 4 nm and 47 ± 4 nm, respectively. The ratios between these particular distances report on specific growth rate. From acidic to near neutral conditions at a constant residence time, the ratio l_{200} / l_{020} is reduced from 2.8 to 1.2, l_{002} / l_{020} from 2.3 to 1.2 whereas l_{200} / l_{002} shows a slight decrease from 1.2 to 1.0.

Table 2: Refined parameters and residuals from the Rietveld refinement using spherical harmonic peak shape functions. Calculation error values are mentioned in brackets.

Sample name	**S2.9**	**S3.5**	**S3.9**	**S6.7**
a (nm)	0.2868 (1)	0.2869 (1)	0.2868(1)	0.2868 (1)
b (nm)	1.2225 (1)	1.2221 (2)	1.2222 (1)	1.2219 (1)
c (nm)	0.3693 (1)	0.3694 (1)	0.3693 (1)	0.3694 (1)
R_{wp} (%)	9	8	10	11
l_{200} (nm)	28 (5)	19 (4)	17 (3)	47 (4)
l_{020} (nm)	10 (2)	12 (2)	10 (2)	39 (4)
l_{002} (nm)	23 (6)	18 (4)	17 (3)	47 (4)
l_{200} / l_{020}	2.8	1.6	1.8	1.2

l_{200} / l_{002}	1.2	1.1	1.0	1.0
l_{002} / l_{020}	2.3	1.5	1.8	1.2

Considering only a decrease of the pH, a preferential growth may be underlined along the [100] and [001] directions compared to the [010] one. In addition, crystallite dimensions, measured on TEM images (figure 2), of S3.5 powder with l_{200}, l_{020} and l_{002} of 19 ± 4 nm, 12 ± 2 nm and 18 ± 4 nm, respectively, agreed with a non-significant impact of the residence time on particle growth.

Acidic conditions have led to hexagonal platelets whereas rhombic grains are produced in near neutral solutions. Morphology modification is correlated to pH and so is the variation of nitrates in the solution.

3.2 Adsorption of nitrates

Modification of boehmite morphology can be obtained through anisotropic adsorption of chemical species, nitrates for instance. He *et al.* characterized sulfates adsorption on boehmite particles using Raman spectroscopy [32]. In the case of a sulfate H-bonded complex, a sulfate would not form a direct chemical bond with the surface and the vibrational spectrum is very similar to the spectra of sulfate in solution. Raman spectroscopy appears to be a suitable technique to analyse chemical bonds of adsorbed species thanks to its high sensitivity to molecule vibration. The low wavenumber region Raman spectra of the different boehmite samples is reported in Figure 5. The 400 – 800 cm^{-1} region consists of the hydroxyl translation modes. In particular, the most intense peak at 359 cm^{-1} corresponds to the A_g fully symmetric mode due to the movement of aluminium and oxygen atoms parallel to the [010] direction [33]. The AlO_6 octahedron structure causes two peaks at 494 and 674 cm^{-1} [34,35]. The small and sharp peak at 1049 cm^{-1} which is slightly intense for S2.9 and S3.9 and almost extinct for S6.7 is attributed to NO_3^- vibrations [26,33]. Although Raman spectroscopy gives qualitative information, this peak confirmed the presence of nitrates at the boehmite surfaces, especially on S2.9 and S3.9.

A further study at high wavenumber was performed. Results are presented in Figure 6. This region exhibited up to four bands at 3078, 3219, 3340, 3515 cm^{-1} and eventually a shoulder at 3561 cm^{-1}. The two first peaks characterized the hydroxyl stretching vibrations within boehmite structure and are observable for all the samples [25,34,35].

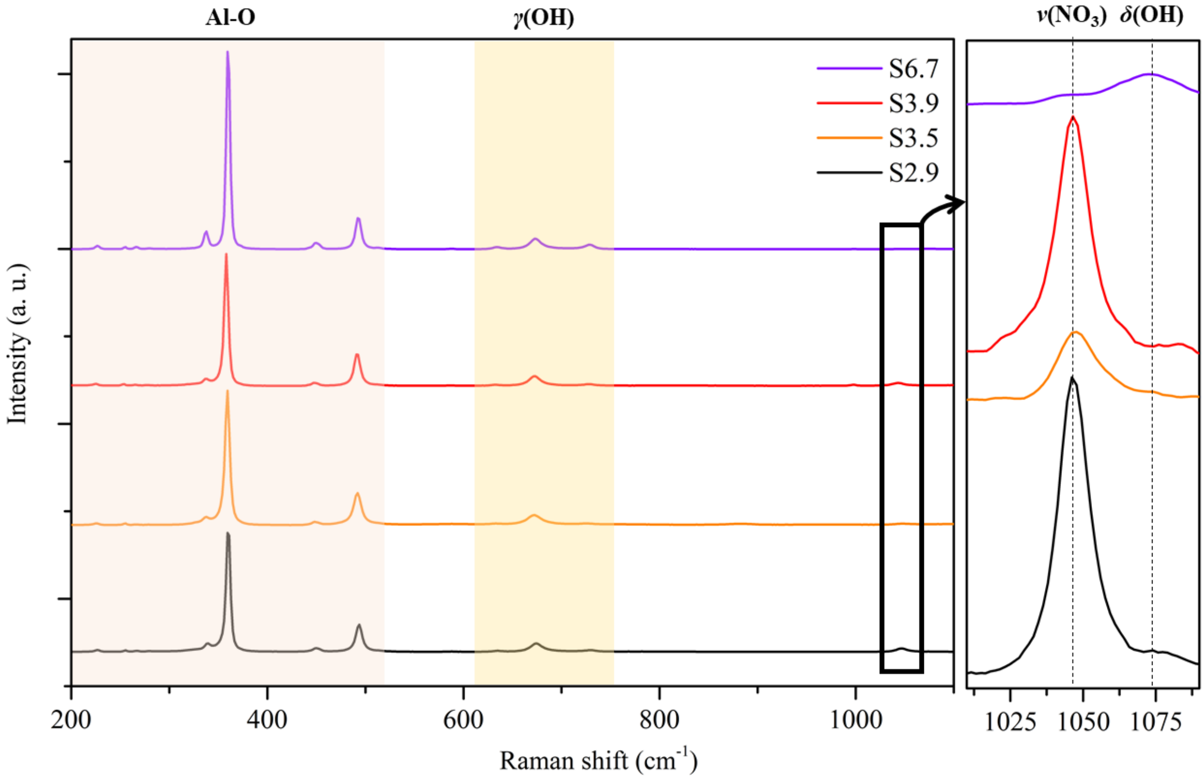

Figure 5: Raman spectra of the low wavenumber region of S2.9, S3.5, S3.9 and S6.7; on the left, from 200 to 1200 cm^{-1}; on the right, a focus on the 1020 - 1080 cm^{-1} region. Each part of the spectra is described with its corresponding assignment.

The assignment above 3300 cm^{-1} is extremely complex because of the intricate hydrogen bonding network [36]. This region is associated with the stretching vibrations of surface OH groups or residual water on the surfaces [25,37]. Bands at 3340, 3515 and 3561 cm^{-1} are displayed for S2.9 and more particularly for S3.5. On the top of Figure 6, a spectrum of a boehmite sample synthesized in a batch reactor using gibbsite $Al(OH)_3$ as a precursor and so without nitrates is depicted. This spectrum shows the structural hydroxyl stretching vibrations between 3000 and 3300 cm^{-1} but does not display any bands at higher frequency. Consequently, bands above 3300 cm^{-1} may have a link with surface hydroxynitrates. Observations done by Herzog-Cance *et al.* who studied the nitric acid autoprotolysis using Raman spectroscopy confirmed the substantial correlation between these bands and nitrates [38]. Thus, the band at 3340 cm^{-1} may correspond to the stretching contribution of weakly bonded HNO_3 also named as “free” nitric acid. The greatest band at 3515 cm^{-1} could be attributed to the stretching vibration of water associated with nitric acid molecules through the

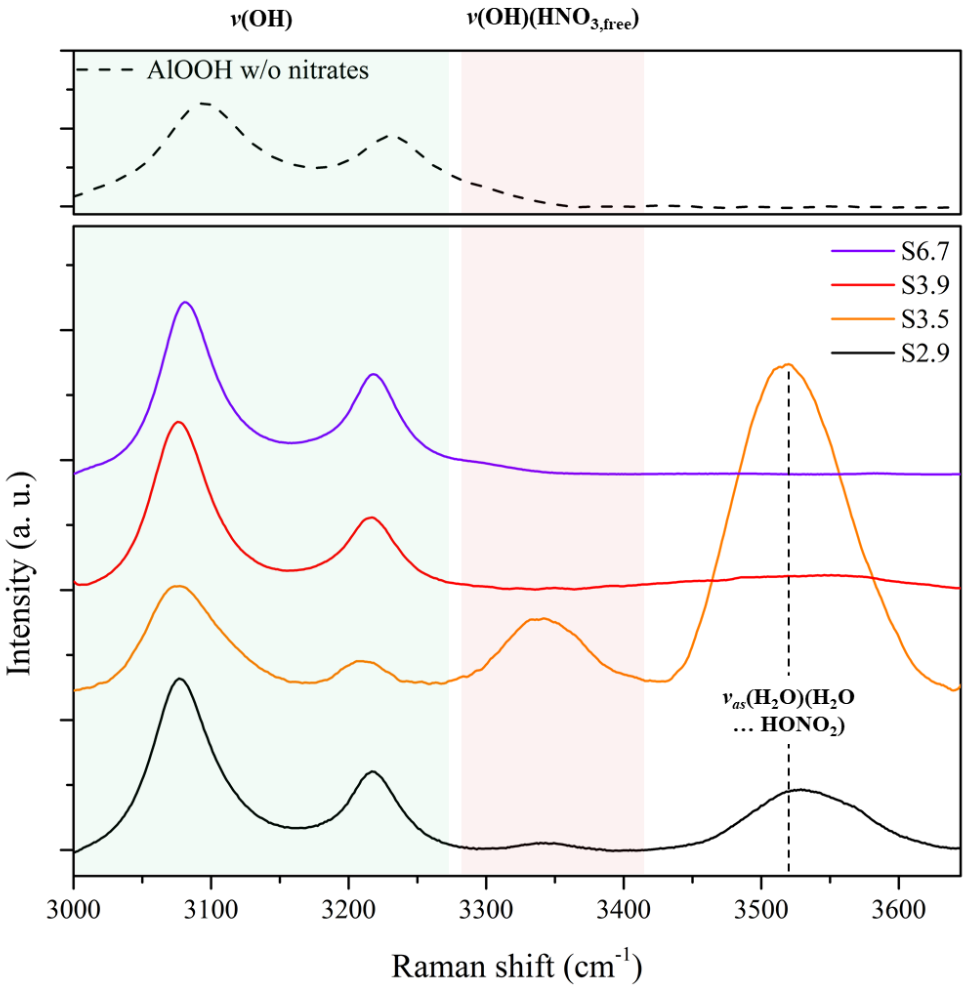

Figure 6: Raman spectra of the high wavenumber region from 3000 to 3650 cm^{-1} of; on the top, a boehmite sample synthesized without nitrates; on the bottom, S2.9, S3.5, S3.9 and S6.7. Each part of the spectra is described with its corresponding assignment.

molecular association H_2O … $HONO_2$ produced from the dissociation of the HNO_3 molecule [38]. The shoulder at 3561 cm^{-1} may assimilate to differently bonded water molecules. Assignments of the Raman spectra indicated a strong adsorption of nitrate species, especially in acidic conditions. Bands correlated to nitrate signatures almost disappear for S3.9 and are inexistent for S6.7. Raman spectroscopy of S3.5 at a longer residence time has demonstrated many signatures of nitrates under various forms.

Nitrate adsorption occurred more under acidic conditions as shown in Raman spectroscopy results, leading to the formation of hexagonal particles. The next part will deal with the interaction between these specific morphologies and the adsorption of water molecules.

3.3 Adsorbed water determination

Nguefack *et al.* developed a model to investigate adsorbed water content on boehmite crystallites based on free sites available on each facet [39]. They obtained the maximum adsorption capability by expanding the coordination number of surface aluminium atoms to six and surface oxygen atoms to four. Stoichiometric water content adsorption x is calculated by dividing the number of free sites by the total number of atoms in the crystal. To estimate the free site number, the model uses the A.C.S. and lattice parameters refined from the Rietveld method. The corresponding results are summarized in Table 3.

Table 3: Determination of the relative facet areas of the three mains faces (100), (010) and (001) and of the overall adsorbed water calculated using the model of Nguefack et al. [38].

Sample name	**S2.9**	**S3.5**	**S3.9**	**S6.7**
$S_{(100)}$ (%)	20	26	30	31
$S_{(010)}$ (%)	56	45	41	38
$S_{(001)}$ (%)	24	28	29	31
$AlOOH.xH_2O$	**0.16**	**0.18**	**0.21**	**0.07**

As stated above, the (010) facet is dominant with a relative surface area between 56 % and 38 % for S2.9 and S6.7, respectively. However, the basal surface decreases when the pH becomes more neutral to the benefit of the (100) and (001) facets. This is in agreement with the observation of the Rietveld refinement with the inhibition of (100) and (001) facets in acidic conditions. Stoichiometric water content increased from 0.16 to 0.21 following the inverse of the (010) relative facet area.

S3.5 sample follows the same tendency and does not show a significant effect of residence time. Bigger crystallites obtained for S6.7 have less adsorption sites in proportion to the total number of atoms in the crystal and so less water is adsorbed following this model.

To sum up, a raise of the pH from 2.9 to 3.9 is followed by a slight increase of water content whereas a further increase of the pH to 6.7 generated a drastic reduction of water content.

As explained in the introduction, two possibilities have been suggested for the location of water. The first assumption was inside the structure along the b-axis. However, the Rietveld refinement revealed a restricted variation of the crystal dimension along the b-axis, insufficient to insert any atoms within the structure. Consequently, the excess of water is probably adsorbed on the crystal surfaces.

3.4 Investigation of surface species and their chemical environment

XPS survey scans, shown in Figure 7, exhibit very clean samples with mostly Al and O atoms and the adventitious C between 4.2 and 9.7 at. %. This is confirmed by the Al/O ratio equal to 0.5. In addition, no significant shift of the Al_{2p} binding energies is observed with a position at approximately 74.0 and 74.1 eV meaning that the oxidation state of Al atoms is stable for all the samples.

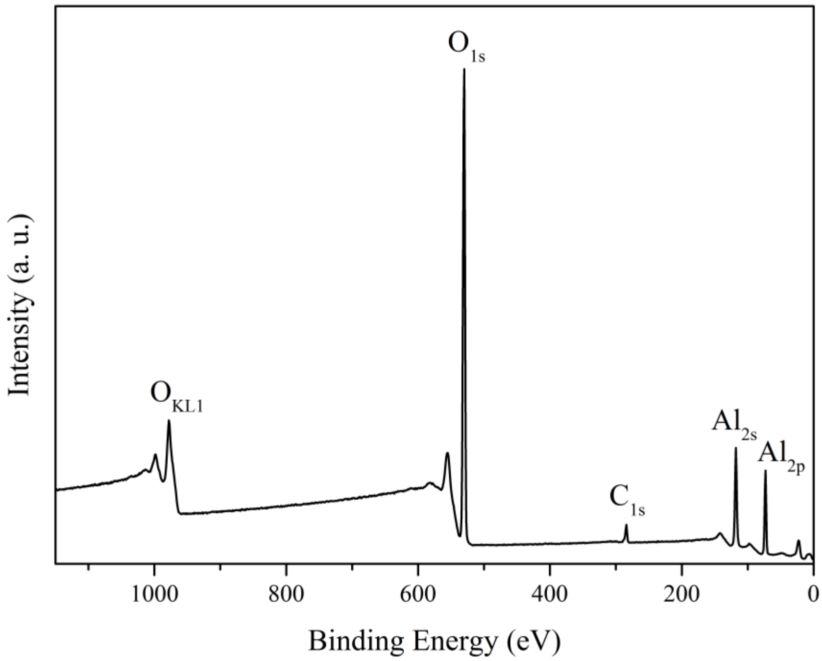

Figure 7: XPS survey spectrum of the boehmite S2.9 sample.

Table 4: Summary of the C_{1s}, Al_{2p} and O_{1s} spectra description with the full width at half maximum (FWHM), the atomic proportions of each environment and the ratio between

Sample name		S2.9	S3.5	S3.9	S6.7
FWHM (± 0.1 eV)					
Al_{2p}		1.8	1.4	1.5	1.5
O_{1s}	*Al-O-Al*	1.6	1.4	1.5	1.5
	Al-OH	1.9	1.6	1.7	1.8
	Ads. H_2O	1.9	1.4	1.7	1.8
Atomic proportions (± 0.1 %)					
C_{1s}		6.2	4.2	6.5	9.7

Al$_{2p}$		31.3	33.3	31.3	29.9
O$_{1s}$	*Al-O-Al*	18.3	25.7	19.8	20.5
	Al-OH	26.6	30.7	22.1	24.8
	Ads. H_2O	17.7	6.1	20.4	15.1

Ratio				
Al$_{2p}$/O$_{1s}$	0.5	0.5	0.5	0.5
O$_{1s}$ (*Ads.* H_2O*/Al-O-Al*)	1.0	0.2	1.0	0.7
O$_{1s}$ (*Al-OH/Al-O-Al*)	1.5	1.2	1.1	1.2

Figure 8 exhibits the high-resolution O_{1s} spectra of the four samples fitted into three components. The first contribution at 530.4 ± 0.1 eV is attributed to the Al-O-Al structure, the

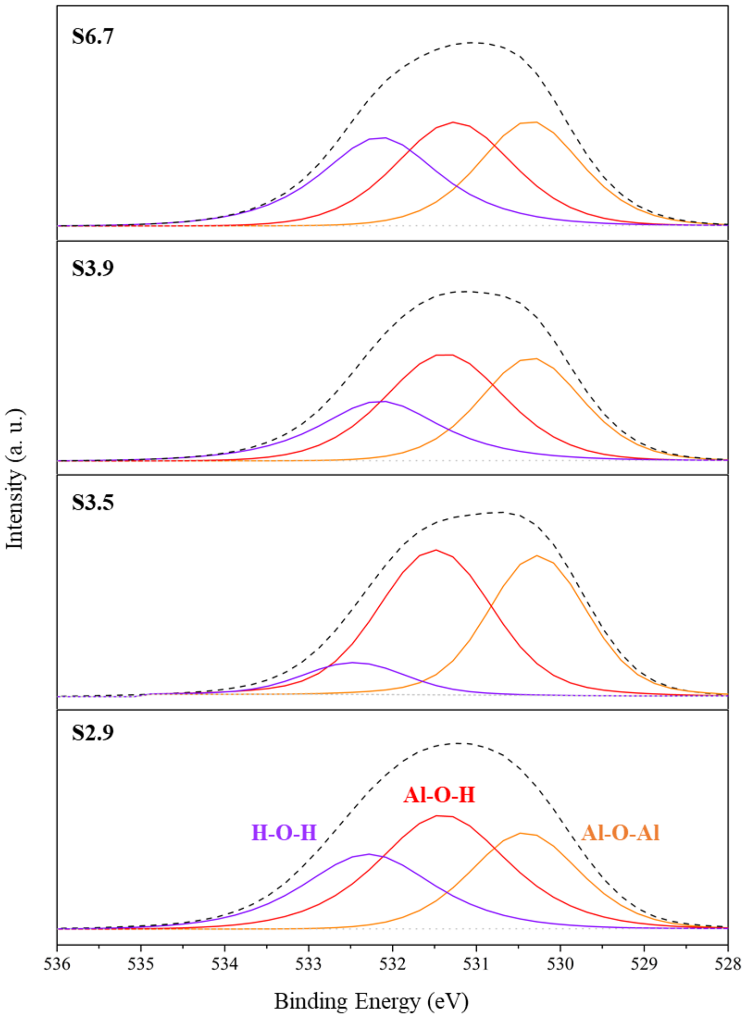

Figure 8: Fitted XPS O_{1s} spectra of S2.9, S3.5, S3.9 and S6.7 into three contributions: Al-O-Al structure in orange, structural hydroxyls in red and adsorbed water in purple.

second one at 531.4 ± 0.1 eV to the Al-O-H within the crystal and the third one between 532.2 ± 0.1 eV and 532.5 ± 0.1 eV to the adsorbed water on the surface [40]. Peak broadening provides information on the structure disorder. The wider is the peak broadening, the more disordered the local atom environment is. Al_{2p} and O_{1s} peak broadenings follow the same trend and decrease with pH. For instance, Al_{2p} peak broadening changes from 1.8 eV to 1.5 eV for S2.9 and S6.7, respectively. S3.5 sample exhibits the more ordered structure with the lowest peak broadening for aluminium. This means that an increase in the residence time to 60 s does not promote the particle growth but improves the local structure order. The contribution of ads. H_2O revealed some variations of the adsorbed water on the boehmite surfaces. Indeed, S3.9 has the highest adsorbed water contribution with 20.4 at.%. In comparison, the lowest is contained on S3.5 surfaces with only 6.1 at.%. The study of the ratios between these contributions makes it possible to get rid of the impurity effects such as carbon. The adsorbed water content is quite similar for both S2.9 and S3.9 with a ratio $\frac{O_{1s}\,(Ads.\ H_2O)}{O_{1s}\,(Al-O-Al)}$ close to 1 and is reduced down to 0.7 for S6.7 at high pH.

However, an increase in the residence time with S3.5 proposed to reduce significantly this ratio and so the adsorbed water content to 0.2. These observations are almost in agreement with the adsorption site calculation (Table 3) except for S3.5. The ratio $\frac{O_{1s}\,(Al-OH)}{O_{1s}\,(Al-O-Al)}$ is expected to be nearly 1 according the AlOOH chemical formula [40]. This ratio is about 1.2 for S3.5, S3.9 and S6.7 and raised to 1.5 for S2.9, highlighting an excess of surface hydroxyls in these conditions. The depth probed by XPS (≈ 3 to 5 nm) coupled with crystallite thickness near 10 nm for S2.9, S3.5 and S3.9 likely might overestimate the adsorbed water and surface hydroxyl compared to thicker crystallites of S6.7.

Even if the assignment of ^{1}H resonance lines is very challenging, ^{1}H Solid-State NMR spectra of the S2.9 and S3.5 samples confirmed the observations done using XPS and summarized in Figure 8.

In Figure 9, the ^{1}H MAS NMR spectrum of S3.5 can be described as the sum of four main resonance lines centered at 1.2, 3.5, 7.1 and 10.4 ppm. Peaks at 7.1 and 10.4 ppm are tentatively assigned to structural octahedral Al_2OH sites which involve different strength of bonds while the one located at 3.5 ppm is attributed to octahedral AlOH sites [41]. The narrow resonance line at 1.2 ppm is often referred as another contribution of octahedral AlOH sites. The slight variation in ^{1}H NMR shifts between different authors is likely due to difference in morphology of boehmite particles [42]. In comparison, an additional peak at 4.7 ppm is exhibited for the sample S2.9. This contribution counting for 25 % of the overall resonance area coincides undoubtedly to the protons of “physisorbed” water on boehmite particles [41,42].

As stated previously, A.C.S. plays an important role but are insufficient to explain all the involved surface reactions. Especially, the local environment order would appear to have a major impact.

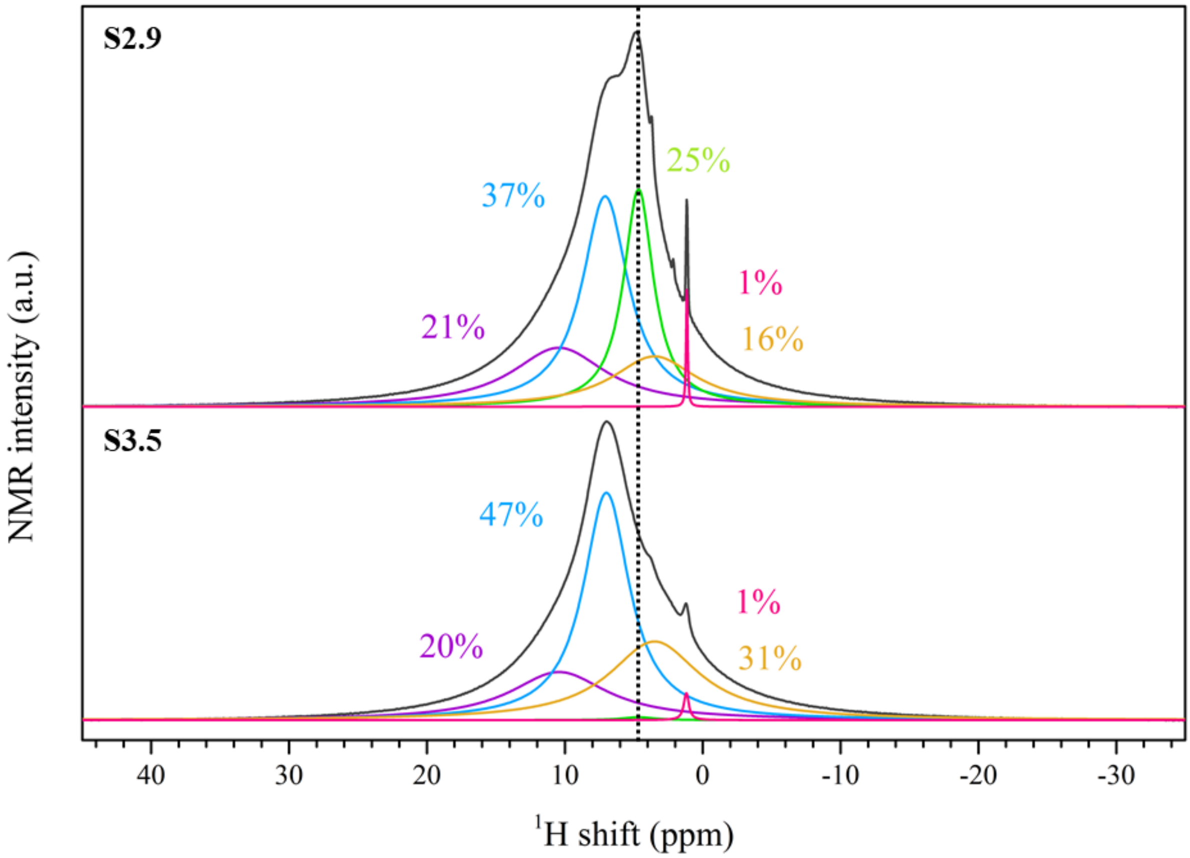

Figure 9: ^{1}H MAS NMR spectra of boehmite samples S2.9 and S3.5. Fitted curves with the respective contributions in percentage are presented. The dashed line corresponds to the weakly bonded water.

4. Discussion

Firstly, the discussion is focused on the effect of pH considering the samples S2.9, S3.9 and S6.7. pH has a great impact on the fluctuation of the boehmite particle morphology synthesized using the continuous supercritical hydrothermal process. Indeed, a highly acidic pH or a neutral one will give anisotropic hexagonal-plate and rhombic particles, respectively. Boehmite synthesis, described by the chemical reaction below, produces also HNO_3 [43].

$$Al(NO_3)_3 + 2H_2O = AlOOH + 3HNO_3 \#(1)$$

These HNO_3 molecules may adsorb on boehmite particle surfaces. Raman spectroscopy underlined the strong presence of nitrates on the hexagonal-plate boehmite powders (Figure 5 and Figure 6). In acidic conditions, the anion adsorption is favored due to the positive charges at the boehmite surface determined with a zeta potential study considering an isoelectric point of boehmite between 7 and 9.2 depending on the morphology and the particle size [44,45]. On the contrary, at near neutral pH, there is no adsorbed anions leading to no or a little preferential growth and so to large rhombic particles. The less acidic the solution is, the less anion adsorption will occur. Furthermore, the anion adsorption may be surface-dependent. Nitrates seem to adsorb preferentially on (020) surface resulting in a preferential growth along the [001] and mostly [100] directions. Consequently, the relative (020) surface is increased compared to the edge surfaces (Table 3).

According to the model developed by Nguefack *et al.*, the less prominent the (020) relative surface is, the less water is adsorbed on the boehmite surfaces. The XPS results tend to this conclusion too with a strong reduction of the adsorbed water content for pH from 2.9 to 6.7. This is directly linked to the crystal structure of boehmite. As the octahedral double layer interactions are weak in the boehmite structure, the crystal is easily cleaved between these layers causing (010) surfaces to be covered by hydroxyl groups [11,12]. However, the difference is not significant between pH values equal to 2.9 and 3.9, which could be explained by a reduction of the available sites for water adsorption. Even if the sample S2.9 has more adsorption sites, they are probably mostly filled with nitrate species. In addition, a very low pH seems to promote a dissociative adsorption of water resulting in more surface hydroxyl groups.

Secondly, the residence time does not significantly influence the morphology. In acidic conditions, hexagonal-plate particles with the same range of size were synthesized at longer residence time (60 s instead of 20 s). Surprisingly, this sample exhibits a very small adsorbed water content, lower than the one of sample done at pH 6.7, which is totally at odds with the model of Table 3. The increase of the residence time implies a real improvement of the local structure environment (Table 4, see FWHM). In this case, oxygen with a free orbital will form a ligand between an aluminium atom and the non-reacted nitrates in solution. Thus, nitrate hydroxyls such as $Al_2O_2(OH)NO_3$ can be formed at the surfaces preventing further adsorption of water [46]. These species may have the time to be stabilized and so to reduce the local disorder.

Surfaces may be fully adsorbed by H-bonded liquid HNO_3. During the synthesis, produced nitric acid in the fluid will react with the surface of the particles and especially at low pH. The strong peak at 3515 cm^{-1} in Figure 6 may prove that the molecular association H_2O … $HONO_2$ is weakly bonded at the surface of boehmite. The intensity of this peak differs from the small content of adsorbed water observed using XPS and ^1H MAS NMR spectroscopy. As a result, the residence time increase may promote the adsorption of hydroxynitrates combined with the one of liquid HNO_3 leading to the full filling of the free adsorption sites of boehmite.

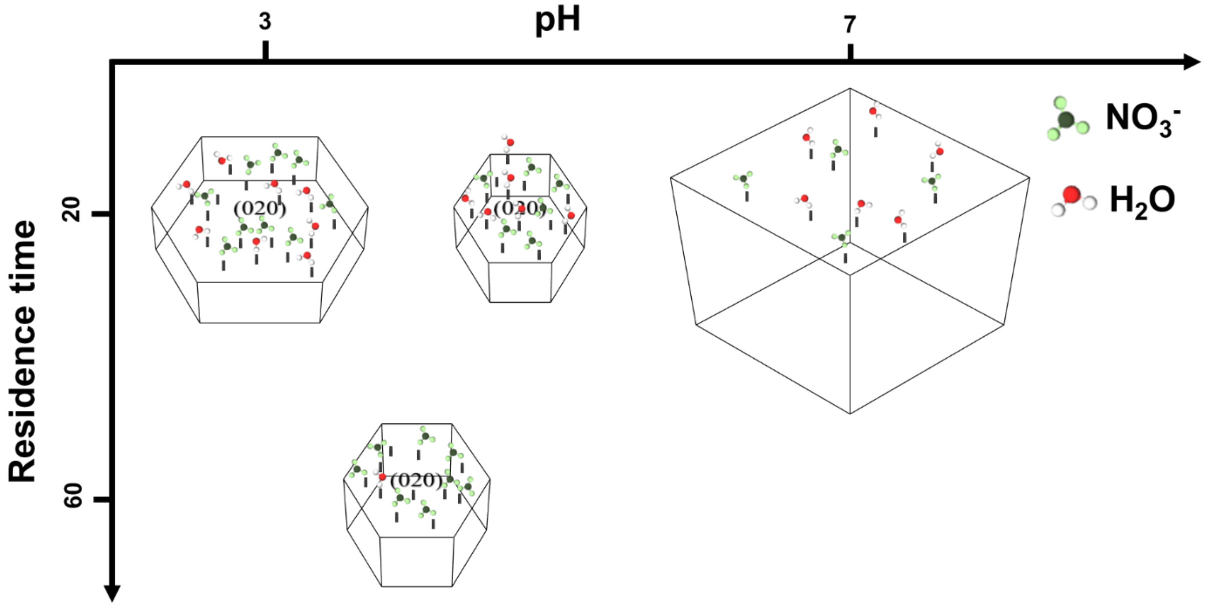

Figure 10: Schematic representation of the adsorption phenomena on different morphologies of boehmite.

The scheme displayed in Figure 10 summarizes the discussion.

From the pH variation, two factors are pointed out on the adsorbed water modification. A weakly alkaline pH will give rhombic grains with a little relative (020) surface. This will lead to a reduced adsorbed water content validated by XPS results (Figure 8).

In the case of an acidic environment, it is more complex. The decrease of the pH will allow the production of hexagonal-plate grains associated with an increase of the relative (020) surface area (Table 3). Nevertheless, the more acid the environment is, the more nitrates will be adsorbed (Figure 5). These molecules may block the further adsorption of water at the surface of boehmite particles.

Decrease of the available adsorption sites at high residence time is due to the improvement of the intricate structure with the hydroxynitrates and of the HNO_3 content at the surface.

Finally, the prediction of the adsorbed water quantity is very tricky. Indeed, it involves complex interdependent phenomena linking the growth along specific directions, anisotropic surface reactions of chemical species such as anions and available adsorption free sites.

5. Conclusion

This study investigated the adsorption of water on various morphologies of boehmite particles synthesized using the continuous supercritical hydrothermal synthesis. The use of this process allowed to synthesize pure and crystalline submicrometer boehmite particles. pH modification from 2.9 to 6.7 offered a way to tune the particle morphologies from hexagonal platelets to rhombic grains and the sizes of the particles. In fact, the anisotropic nature of boehmite results in a surface-dependent anion adsorption. Nitrates were adsorbed preferentially on the (020) surface leading to a preferential growth along [001] and mostly [100] directions.

Our results showed that the adsorption of water cannot be characterized only by a morphological analysis. It depends substantially on two phenomena. First, the more ordered the crystal structure is, the less the adsorbed water will be. XPS analysis combined with ^{1}H Solid-State NMR experiments have effectively highlighted the very small amount of adsorbed water on well-ordered boehmite particles. Secondly, in acidic conditions, anions such NO_3^- are attracted to the boehmite surfaces leading to the diminution of the adsorption sites as shown by Raman spectroscopy.

Then interaction between the boehmite morphology and the adsorption of water is very difficult to be predicted because it is correlated with different parameters such as crystallite size, structural order and other adsorbed species such as nitrates.

Declaration of Competing Interest

The authors declare that they have no known competing financial interests or personal relationships that could have appeared to influence the work reported in this paper.

Acknowledgement

The authors would like to thank the “Agence de l’Innovation de Défense (AID)” and the Safran company for their financial support. They would also like to thank E. Lebraud and B. Dusolle both from ICMCB laboratory for their respective contributions for the XRD analyses and for the graphical abstract.

References

[1] C. Aymonier, A. Loppinet-Serani, H. Reverón, Y. Garrabos, F. Cansell, Review of supercritical fluids in inorganic materials science, J. Supercrit. Fluids. 38 (2006) 242–251. https://doi.org/10.1016/j.supflu.2006.03.019.

[2] C. Aymonier, G. Philippot, A. Erriguible, S. Marre, Playing with chemistry in supercritical solvents and the associated technologies for advanced materials by design, J. Supercrit. Fluids. 134 (2018) 184–196. https://doi.org/10.1016/j.supflu.2017.12.021.

[3] A. Takagaki, J. Chul Jung, S. Hayashi, Solid Lewis acidity of boehmite γ-AlO(OH) and its catalytic activity for transformation of sugars in water, RSC Adv. 4 (2014) 43785–43791. https://doi.org/10.1039/C4RA08061K.

[4] F. Granados-Correa, J. Jiménez-Becerril, Chromium (VI) adsorption on boehmite, J. Hazard. Mater. 162 (2009) 1178–1184. https://doi.org/10.1016/j.jhazmat.2008.06.002.

[5] P. Li, S. Zheng, P. Qing, Y. Chen, L. Tian, X. Zheng, Y. Zhang, The vanadate adsorption on a mesoporous boehmite and its cleaner production application of chromate, Green Chem. 16 (2014) 4214–4222. https://doi.org/10.1039/C4GC00897A.

[6] H. Zhang, P. Li, Z. Wang, X. Zhang, S. Zheng, Y. Zhang, *In Situ* Synthesis of γ-AlOOH and Synchronous Adsorption Separation of V(V) from Highly Concentrated Cr(VI) Multiplex Complex solutions, ACS Sustain. Chem. Eng. 5 (2017) 6674–6681. https://doi.org/10.1021/acssuschemeng.7b00918.

[7] Z. Wang, J. Gong, J. Ma, J. Xu, In situ growth of hierarchical boehmite on 2024 aluminum alloy surface as superhydrophobic materials, RSC Adv. 4 (2014) 14708–14714. https://doi.org/10.1039/C4RA00160E.

[8] V. Vatanpour, S.S. Madaeni, L. Rajabi, S. Zinadini, A.A. Derakhshan, Boehmite nanoparticles as a new nanofiller for preparation of antifouling mixed matrix membranes, J. Membr. Sci. 401–402 (2012) 132–143. https://doi.org/10.1016/j.memsci.2012.01.040.

[9] J. Zhang, Q. Ji, P. Zhang, Y. Xia, Q. Kong, Thermal stability and flame-retardancy mechanism of poly(ethylene terephthalate)/boehmite nanocomposites, Polym. Degrad. Stab. 95 (2010) 1211–1218. https://doi.org/10.1016/j.polymdegradstab.2010.04.001.

[10] A. Boumaza, L. Favaro, J. Lédion, G. Sattonnay, J.B. Brubach, P. Berthet, A.M. Huntz, P. Roy, R. Tétot, Transition alumina phases induced by heat treatment of boehmite: An X-ray diffraction and infrared spectroscopy study, J. Solid State Chem. 182 (2009) 1171–1176. https://doi.org/10.1016/j.jssc.2009.02.006.

[11] X. Bokhimi, J.A. Toledo-Antonio, M.L. Guzmán-Castillo, B. Mar-Mar, F. Hernández-Beltrán, J. Navarrete, Dependence of Boehmite Thermal Evolution on Its Atom Bond Lengths and Crystallite Size, J. Solid State Chem. 161 (2001) 319–326. https://doi.org/10.1006/jssc.2001.9320.

[12] X. Bokhimi, J.A. Toledo-Antonio, M.L. Guzmán-Castillo, F. Hernández-Beltrán, Relationship between Crystallite Size and Bond Lengths in Boehmite, J. Solid State Chem. 159 (2001) 32–40. https://doi.org/10.1006/jssc.2001.9124.

[13] B.R. Baker, R.M. Pearson, Water content of pseudoboehmite: A new model for its structure, J. Catal. 33 (1974) 265–278. https://doi.org/10.1016/0021-9517(74)90270-X.

[14] B.C. Lippens, Structure and texture of aluminas, Technical University of Delft, 1961.

[15] M.L. Guzmán-Castillo, X. Bokhimi, A. Toledo-Antonio, J. Salmones-Blásquez, F. Hernández-Beltrán, Effect of Boehmite Crystallite Size and Steaming on Alumina Properties, J. Phys. Chem. B. 105 (2001) 2099–2106. https://doi.org/10.1021/jp001024v.

[16] P. Raybaud, M. Digne, R. Iftimie, W. Wellens, P. Euzen, H. Toulhoat, Morphology and Surface Properties of Boehmite (γ-AlOOH): A Density Functional Theory Study, J. Catal. 201 (2001) 236–246. https://doi.org/10.1006/jcat.2001.3246.

[17] T. Adschiri, K. Kanazawa, K. Arai, Rapid and Continuous Hydrothermal Synthesis of Boehmite Particles in Subcritical and Supercritical Water, J. Am. Ceram. Soc. 75 (1992) 2615–2618. https://doi.org/10.1111/j.1151-2916.1992.tb05625.x.

[18] P.H. Hsu, Effect of salts on the formation of bayerite versus pseudo-boehmite, Soil Sci. 103 (1967) 101–110.

[19] R. Tettenhorst, Crystal Chemistry of Boehmite, Clays Clay Miner. 28 (1980) 373–380. https://doi.org/10.1346/CCMN.1980.0280507.

[20] Y. Hakuta, H. Ura, H. Hayashi, K. Arai, Effects of hydrothermal synthetic conditions on the particle size of γ-AlO(OH) in sub and supercritical water using a flow reaction system, Mater. Chem. Phys. 93 (2005) 466–472. https://doi.org/10.1016/j.matchemphys.2005.03.047.

[21] T. Fujii, S. Kawasaki, A. Suzuki, T. Adschiri, High-Speed Morphology Control of Boehmite Nanoparticles by Supercritical Hydrothermal Treatment with Carboxylic Acids, Cryst. Growth Des. 16 (2016) 1996–2001. https://doi.org/10.1021/acs.cgd.5b01584.

[22] V. Musumeci, P.S. Camacho, K. Xu, P.J.M. Monteiro, J.S. Dolado, C. Aymonier, Sub- and supercritical hydrothermal route for the synthesis of xonotlite nanofibers for application to green concrete materials, J. Supercrit. Fluids. 184 (2022) 105583. https://doi.org/10.1016/j.supflu.2022.105583.

[23] J. Rodriguez-Carvajal, FullProf Suite, (2005).

[24] J. Rodríguez-Carvajal, Study of Micro-Structural Effects by Powder Diffraction Using the Program FULLPROF, Lab. Léon Brillouin CEA-CNRS. 91191 (2003) 11.

[25] H.D. Ruan, R.L. Frost, J.T. Kloprogge, Comparison of Raman spectra in characterizing gibbsite, bayerite, diaspore and boehmite, J. Raman Spectrosc. 32 (2001) 745–750. https://doi.org/10.1002/jrs.736.

[26] J.T. Kloprogge, R.L. Frost, Raman microscopy study of basic aluminium nitrate, Spectrochim. Acta. A. Mol. Biomol. Spectrosc. 55 (1998) 163–169. https://doi.org/10.1016/S1386-1425(98)00178-4.

[27] D. Massiot, F. Fayon, M. Capron, I. King, S. Le Calvé, B. Alonso, J.-O. Durand, B. Bujoli, Z. Gan, G. Hoatson, Modelling one- and two-dimensional solid-state NMR spectra, Magn. Reson. Chem. 40 (2002) 70–76. https://doi.org/10.1002/mrc.984.

[28] N. Lock, P. Hald, M. Christensen, H. Birkedal, B.B. Iversen, Continuous flow supercritical water synthesis and crystallographic characterization of anisotropic boehmite nanoparticles, J. Appl. Crystallogr. 43 (2010) 858–866. https://doi.org/10.1107/S0021889810019187.

[29] T. Voisin, A. Erriguible, C. Aymonier, A new solvent system: Hydrothermal molten salt, Sci. Adv. 6 (2020). https://doi.org/10.1126/sciadv.aaz7770.

[30] E. Duverger-Nédellec, T. Voisin, A. Erriguible, C. Aymonier, Unveiling the complexity of salt(s) in water under transcritical conditions, J. Supercrit. Fluids. 165 (2020) 104977. https://doi.org/10.1016/j.supflu.2020.104977.

[31] X. Zhang, P.L. Huestis, C.I. Pearce, J.Z. Hu, K. Page, L.M. Anovitz, A.B. Aleksandrov, M.P. Prange, S. Kerisit, M.E. Bowden, W. Cui, Z. Wang, N.R. Jaegers, T.R. Graham, M. Dembowski, H.-W. Wang, J. Liu, A.T. N'Diaye, M. Bleuel, D.F.R. Mildner, T.M. Orlando, G.A. Kimmel, J.A. La Verne, S.B. Clark, K.M. Rosso, Boehmite and Gibbsite Nanoplates for the Synthesis of Advanced Alumina Products, ACS Appl. Nano Mater. 1 (2018) 7115–7128. https://doi.org/10.1021/acsanm.8b01969.

[32] T. He, L. Xiang, S. Zhu, Hydrothermal Preparation of Boehmite Nanorods by Selective Adsorption of Sulfate, Langmuir. 24 (2008) 8284–8289. https://doi.org/10.1021/la8008514.

[33] C.J. Doss, R. Zallen, Raman studies of sol-gel alumina: Finite-size effects in nanocrystalline AlO(OH), Phys. Rev. B. 48 (1993) 15626–15637. https://doi.org/10.1103/PhysRevB.48.15626.

[34] A.B. Kiss, G. Keresztury, L. Farkas, Raman and i.r. spectra and structure of boehmite (γ-AlOOH). Evidence for the recently discarded D172h space group, Spectrochim. Acta Part Mol. Spectrosc. 36 (1980) 653–658. https://doi.org/10.1016/0584-8539(80)80024-9.

[35] J. Yang, R.L. Frost, Synthesis and Characterization of Boehmite Nanofibers, Res. Lett. Inorg. Chem. 2008 (2008) 1–4. https://doi.org/10.1155/2008/602198.

[36] A.J. Casella, T.G. Levitskaia, J.M. Peterson, S.A. Bryan, Water O–H Stretching Raman Signature for Strong Acid Monitoring via Multivariate Analysis, Anal. Chem. 85 (2013) 4120–4128. https://doi.org/10.1021/ac4001628.

[37] D. Tunega, H. Pašalić, M.H. Gerzabek, H. Lischka, Theoretical study of structural, mechanical and spectroscopic properties of boehmite (γ-AlOOH), J. Phys. Condens. Matter. 23 (2011) 404201. https://doi.org/10.1088/0953-8984/23/40/404201.

[38] M.-H. Herzog-Cance, A. Potier, J. Potier, Étude, par spectroscopie de vibration, de l'autoprotolyse de l'acide nitrique absolu. Nouvelle interprétation, Can. J. Chem. 63 (1985) 1492–1501. https://doi.org/10.1139/v85-256.

[39] M. Nguefack, A.F. Popa, S. Rossignol, C. Kappenstein, Preparation of alumina through a sol–gel process. Synthesis, characterization, thermal evolution and model of intermediate boehmite, Phys Chem Chem Phys. 5 (2003) 4279–4289. https://doi.org/10.1039/B306170A.

[40] J.T. Kloprogge, L.V. Duong, B.J. Wood, R.L. Frost, XPS study of the major minerals in bauxite: Gibbsite, bayerite and (pseudo-)boehmite, J. Colloid Interface Sci. 296 (2006) 572–576. https://doi.org/10.1016/j.jcis.2005.09.054.

[41] J.J. Fitzgerald, G. Piedra, S.F. Dec, M. Seger, G.E. Maciel, Dehydration Studies of a High-Surface-Area Alumina (Pseudo-boehmite) Using Solid-State ^1H and ^27Al NMR, J. Am. Chem. Soc. 119 (1997) 7832–7842. https://doi.org/10.1021/ja970788u.

[42] P. Paluch, N. Potrzebowska, A.M. Ruppert, M.J. Potrzebowski, Application of 1H and 27Al magic angle spinning solid state NMR at 60kHz for studies of Au and Au-Ni catalysts supported on boehmite/alumina, Solid State Nucl. Magn. Reson. 84 (2017) 111–117. https://doi.org/10.1016/j.ssnmr.2017.01.005.

[43] T. Adschiri, Y. Hakuta, K. Sue, K. Arai, Hydrothermal Synthesis of Metal Oxide Nanoparticles at Supercritical Conditions, J. Nanoparticle Res. 3 (2001) 227–235.

[44] T. He, L. Xiang, S. Zhu, Different nanostructures of boehmite fabricated by hydrothermal process: effects of pH and anions, CrystEngComm. 11 (2009) 1338. https://doi.org/10.1039/b900447p.

[45] M. Pandey, P. Mishra, D. Saha, K. Sengupta, s. S. Islam, Development of Commercial Trace Moisture Sensor: A Detailed Comparative Study on Microstructural

and Impedance Measurements of Two Phases of Alumina, Electron. Mater. Lett. 10 (2014). https://doi.org/10.1007/s13391-013-2196-1.

[46] M.W. Ross, T.C. DeVore, Desorption of Nitric Acid From Boehmite and Gibbsite, J. Phys. Chem. A. 112 (2008) 6609–6620. https://doi.org/10.1021/jp7110555.